Shape optimization for composite materials in linear elasticity

Helmut Harbrecht, Merlin Fallahpour

Departement Mathematik und Informatik
Fachbereich Mathematik
Universität Basel
CH-4051 Basel

Preprint No. 2021-21
December 2021

dmi.unibas.ch

SHAPE OPTIMIZATION FOR COMPOSITE MATERIALS IN LINEAR ELASTICITY

MERLIN FALLAHPOUR AND HELMUT HARBRECHT

Abstract. This article is devoted to the optimal design of the microstructure in composite materials, which are governed by the equations of linear elasticity. To this end, we combine homogenization with shape optimization. In particular, we consider the sensitivity of the homogenized coefficients of the elasticity tensor with respect to the shape of the microstructure. We compute Hadamard's shape gradient and demonstrate the applicability and feasibility of our approach by numerical experiments.

Key words. Linear elasticity, composite materials, homogenization, shape optimization.

1. Introduction

The equations describing the behaviour of materials with elastic properties are widely studied in mechanics. Especially, the simplified case of linear elasticity is of interest. The system of equations considered in this article describes the behaviour of an elastic material subject to surface loads. Our material is considered to be periodically heterogeneous. Specifically, on a microscopic scale, one substance envelops another substance in a periodically repeating pattern. These kind of materials can be produced amongst other techniques by additive manufacturing and find applications in many fields, for example as light weight structures in aeronautics or as synthetic bone material in medical applications.

We aim in this article at optimizing the shapes in the periodically repeating pattern on the microscopic scale. Therefore, an objective function depending on the shapes in the pattern is defined. It describes a desired macroscopic property, which is achieved when the function's minimal solution is found. In order to solve this minimization problem, methods of shape sensitivity analysis are employed. Thus, we are able to compute Hadamard's shape gradient, which allows for the application of gradient based optimization methods to find the optimal shape, compare [7, 17, 24, 20] for example.

Note that the optimal design of periodic structures has already been considered in many works, see [1, 5, 8, 11, 13, 14, 15, 19, 21, 22, 23, 25, 27] for some of the respective results. The methodology used there is mainly based on the forward simulation of the material properties of a given microstructure. Whereas, sensitivity analysis has been used in [3, 9] to compute the derivatives with respect to the side lengths and the orientation of rectangular cavities. In [12], the derivatives with respect to the coefficients of a B-spline parametrization of the cavity have been computed. In [18], the shape derivative has been derived in the context of a level set representation of the inclusion. The novelty of this work is the use of Hadamard's

formula to compute the arbitrary shape derivatives. To this end, we follow the ideas and computations presented in [6, 10] for an elliptic diffusion problem. We emphasize that the numerical results presented in this article are in two spatial dimensions. They serve as a proof of concept and foundation for future works, where we will consider the optimization of three-dimensional problems.

This article is structured as follows. In Section 2, we introduce the system of equations and objects we treat in this article. Especially, we briefly discuss the notation of the computations with tensors. Moreover, homogenization through a multiscale ansatz is performed. The result of the homogenization procedure is a system of equations describing a homogeneous approximation to our material. This new system contains the homogenized elasticity tensor, also called the effective elasticity tensor. Next, the objective function under consideration is introduced. From then on, we consider a composite material, which consists of two intertwined materials with different elastic properties.

In Section 3, the shape derivative of the coefficients of the effective tensor is computed. To this end, we first compute the local shape derivative of the cell functions, then the shape derivative of the material coefficients, and finally the shape derivative of the least squares functional under consideration. These steps are repeated for the special case of a partly hollow material. In the two-dimensional setting, this corresponds to the special case of a perforated plate, while in the three-dimensional setting, we arrive at a scaffold structure.

The implementation in the two-dimensional setting is presented in Section 4. We use a parametrization by a finite Fourier series to represent the sought interface between the two materials in the microcell. Then, we apply parametric finite elements to discretize the state equation under consideration. By means of finite differences we verify our theoretical findings and the implementation.

Section 5 is dedicated to numerical experiments. We optimize for various material parameters the shape of the interface between the two given materials. Especially, we consider nonhomogeneous material parameters, different initial guesses, and also the situtation that there is no interior material. Finally, in Section 6, we state concluding remarks.

2. Notation, homogenization and objective

2.1. **Linear elasticity system.** Consider a fixed, bounded domain $\Omega \subset \mathbb{R}^n$, which is the reference configuration of an elastic body. The structure Ω is clamped on $\Gamma_D \subset \partial\Omega$ and subject to surface loads g in $\Gamma_N \subset \partial\Omega$. Here, Γ_D and Γ_N are assumed to be fixed such that $\Gamma_D \cap \Gamma_N = \emptyset$. The displacement $\boldsymbol{u}$ is then the solution of the system

$$\begin{cases} -\operatorname{div}(\boldsymbol{\sigma}(\boldsymbol{u})) = \boldsymbol{f} & \text{in } \Omega, \\ \boldsymbol{u} = \boldsymbol{0} & \text{on } \Gamma_D, \\ \boldsymbol{\sigma}(\boldsymbol{u})\boldsymbol{n} = \boldsymbol{g} & \text{on } \Gamma_N, \\ \boldsymbol{\sigma}(\boldsymbol{u})\boldsymbol{n} = \boldsymbol{0} & \text{on } \Gamma = \partial\Omega \setminus (\Gamma_D \cup \Gamma_N), \end{cases} \tag{2.1}$$

where the Cauchy stress tensor for the displacement $\boldsymbol{u}$ is defined as

$$\boldsymbol{\sigma}(\boldsymbol{u}) \coloneqq \lambda\,(\nabla \boldsymbol{u} + \nabla \boldsymbol{u}^{\intercal}) + \mu \operatorname{tr}(\nabla \boldsymbol{u})\, id \tag{2.2}$$

with the two Lamé constants $\lambda > 0$ and $\mu > 0$. This system of equations corresponds to the system introduced in [4].

Next, we shall introduce the fourth order elasticity tensor, which allows to express the Cauchy stress tensor in terms of a tensor and of the displacement. To this end, we first introduce some notation for tensors.

2.2. **Tensor notation.** The tensor notation applied in this article follows in wide parts [16]. Let $n \in \mathbb{N}$, a, b, c, d be column vectors in $\mathbb{R}^n$, B, C, D matrices in $\mathbb{R}^{n\times n}$ and id the respective identity matrix. The tensor product for vectors is defined by the relation

$$(a \otimes b)c = (b^\intercal c)a.$$

There hold the following two tensor product relations for matrices which are given by tensor products:

$$(a \otimes b) \otimes (c \otimes d) = a \otimes b \otimes c \otimes d \quad \text{and} \quad (a \otimes b) \odot (c \otimes d) = a \otimes c \otimes d \otimes b.$$

Moreover, there are the transposition operations

$$(a \otimes b \otimes c \otimes d)^\intercal = b \otimes a \otimes d \otimes c \quad \text{and} \quad (a \otimes b \otimes c \otimes d)^{\mathrm{t}} = a \otimes c \otimes b \otimes d.$$

The Frobenius product of two matrices is defined as

$$B : C = \sum_{i,j=1}^{n} b_{ij} c_{ij},$$

and the Frobenius product of a fourth-order tensor $\boldsymbol{A}$ and a matrix B is computed as

$$\boldsymbol{A} : B = \left(\sum_{i,j,k,l=1}^{n} a_{ijkl}(e_i \otimes e_j \otimes e_k \otimes e_l) \right) : \left(\sum_{j,k=1}^{n} b_{jk}(e_j \otimes e_k) \right) = \sum_{i,j,k,l=1}^{n} a_{ijkl} b_{jk} (e_i \otimes e_l).$$

Therefore, we obtain the relations

$$(B \otimes C) : D = BDC \quad \text{and} \quad (B \odot C) : D = B(C : D).$$

With the Lamé constants λ and μ, the fourth-order elasticity tensor $\boldsymbol{A}$, satisfying the relation $\boldsymbol{A} : \nabla \boldsymbol{u} = \boldsymbol{\sigma}(\boldsymbol{u})$, can be expressed as

$$\boldsymbol{A} = \lambda\big((id \otimes id) + (id \otimes id)^{\mathrm{t}}\big) + \mu(id \odot id). \tag{2.3}$$

Especially, with the tensor computation rules above, we find

$$\boldsymbol{A} : B = \lambda\,(B + B^\intercal) + \mu\,\mathrm{tr}\,(B)\,Id,$$

which for $B \coloneqq \nabla u$ corresponds to the Cauchy stress tensor in (2.2).

Remark 1. In some works on linear elasticity, for instance [4] and [9], the elasticity tensor is defined differently. The notation from [16] was chosen in this article since it contains all the objects used in the following pages in a single work. Furthermore, the super-symmetric identity tensor which is introduced in [16] allows to combine the elasticity and strain tensor, often denoted by $\boldsymbol{A}$ and $\boldsymbol{\epsilon}$, respectively, resulting in the elasticity tensor expression (2.3).

Instead of defining the elasticity tensor by means of the Lamé constants λ and μ, we can define it through the elasticity module $E > 0$ and the Poisson ratio $0 < \nu < 1/2$. The elastic module is proportional to the resistance a material opposes to its deformation. The Poisson ratio is a description of the influence of stresses on displacements perpendicular to the specific direction of loading. For soft materials such as rubber it is near 0.5 and for typical solids around 0.2–0.3. The Lamé constants are derived from these two numbers by the formulas

$$\lambda = \frac{E}{(1+\nu)(1-2\nu)} \quad \text{and} \quad \mu = \frac{E}{2(1+\nu)}. \tag{2.4}$$

A fourth-order tensor $\boldsymbol{A}$ is called to be uniformly elliptic if there exists a constant $\alpha > 0$ such that

$$(\boldsymbol{A} : B) : B \geq \alpha B : B \quad \text{for all } B \in \mathbb{R}^{n\times n}. \tag{2.5}$$

This property is always satisfied for the elasticity tensor $\boldsymbol{A}$ defined by E and ν. Thus, we denote the set of admissible elasticity tensors by

$$\mathcal{M}_{E,\nu} \coloneqq \left\{ \boldsymbol{A} \in \mathbb{R}^{n^4} : \boldsymbol{A} \text{ satisfies (2.3), (2.4) with } E > 0 \text{ and } 0 < \nu < 1/2 \right\}.$$

2.3. **The multiscale ansatz and composite materials.** Homogenization is concerned with the situation that the elasticity tensor $\boldsymbol{A}$ is oscillatory. To this end, we denote the unit cell by $Y = [0,1]^n$ and write $\boldsymbol{y} \coloneqq \boldsymbol{x}/\varepsilon$ for any $\boldsymbol{x} \in \Omega$ and $\varepsilon > 0$. We assume $\boldsymbol{A}(\boldsymbol{y})$ to be Y-periodic, satisfying $\boldsymbol{A}(\boldsymbol{y}) \in \mathcal{M}_{E(\boldsymbol{y}),\nu(\boldsymbol{y})}$ for all $\boldsymbol{y} \in Y$ with $E(\boldsymbol{y}) > 0$ and $0 < \nu(\boldsymbol{y}) < 1/2$. Then, in order to approximate the displacement in (2.1), one makes the multiscale ansatz

$$\boldsymbol{u}_\epsilon(\boldsymbol{x}) \coloneqq \boldsymbol{u}_0(\boldsymbol{x},\boldsymbol{y}) + \epsilon \boldsymbol{u}_1(\boldsymbol{x},\boldsymbol{y}) + \epsilon^2 \boldsymbol{u}_2(\boldsymbol{x},\boldsymbol{y}) = \boldsymbol{u}(\boldsymbol{x}) + \mathcal{O}(\epsilon^3). \tag{2.6}$$

With the analogous reasoning as in [2], this ansatz shows that the solution $\boldsymbol{u}_\epsilon$ of the equation

$$-\operatorname{div}\left(\boldsymbol{A}\left(\frac{\boldsymbol{x}}{\epsilon}\right) : \nabla \boldsymbol{u}_\epsilon(\boldsymbol{x}) \right) = \boldsymbol{f}(\boldsymbol{x})$$

can be approximated for $0 < \epsilon \ll 1$ by the solution $\boldsymbol{u}$ of the *homogenized equation*

$$-\operatorname{div}\left(\boldsymbol{A}^* : \nabla \boldsymbol{u}(\boldsymbol{x}) \right) = \boldsymbol{f}(\boldsymbol{x}).$$

To characterize the *effective tensor* $\boldsymbol{A}^*$, we introduce the cell problems

$$\operatorname{div}\Big(\boldsymbol{A}(\boldsymbol{y}) : \big(e_{ij} + \nabla \boldsymbol{w}_{ij}(\boldsymbol{y}) \big) \Big) = \boldsymbol{0}, \quad \boldsymbol{w}_{ij} \in [H^1_{\mathrm{per}}(Y)]^n, \quad (\boldsymbol{w}_{ij}, \mathbb{1})_{[L^2(Y)]^n} = 0, \tag{2.7}$$

where $e_{ij} \coloneqq e_i \otimes e_j$, $i,j = 1,\dots,n$, denotes the basis of matrices. Then, for all $i,j,k,l = 1,\dots,n$, the entries of the effective tensor are given by

$$a^*_{ijkl}(\omega) = \int_Y \Big(\boldsymbol{A}(\boldsymbol{y}) : \big(e_{il} + \nabla \boldsymbol{w}_{il}(\boldsymbol{y}) \big) \Big) : \big(e_{jk} + \nabla \boldsymbol{w}_{jk}(\boldsymbol{y}) \big) \, \mathrm{d}\boldsymbol{y}. \tag{2.8}$$

A composite material consists of two materials with different elastic properties. We model such a material by defining the elastic tensor

$$\boldsymbol{A}(\boldsymbol{y}) = \boldsymbol{A}_1(\boldsymbol{y}) + \big(\boldsymbol{A}_2(\boldsymbol{y}) - \boldsymbol{A}_1(\boldsymbol{y})\big)\mathbb{1}_\omega(\boldsymbol{y}), \tag{2.9}$$

where ω is an open and connected subset of Y. Under the assumption that $\boldsymbol{A}_1(\boldsymbol{y}) \in \mathcal{M}_{E_1(\boldsymbol{y}),\nu_1(\boldsymbol{y})}$ and $\boldsymbol{A}_2(\boldsymbol{y}) \in \mathcal{M}_{E_2(\boldsymbol{y}),\nu_2(\boldsymbol{y})}$ for all $\boldsymbol{y} \in Y$ and $E_1, E_2, \nu_1, \nu_2 \in C^1(Y)$, this is for all choices of ω a piecewise smooth, fourth-order elasticity tensor.

The normal vector $\boldsymbol{n}$ on $\partial\omega$ indicates the direction from the interior of ω to the exterior $Y \setminus \overline{\omega}$. The jump of a function $\boldsymbol{f}$ through the interface $\partial\omega$ at a point $y \in \partial\omega$ is thus given by

$$\big[\boldsymbol{f}(\boldsymbol{y})\big] = \boldsymbol{f}^+(\boldsymbol{y}) - \boldsymbol{f}^-(\boldsymbol{y}) \coloneqq \lim_{t\to 0^+} \boldsymbol{f}\big(\boldsymbol{y} + t\boldsymbol{n}(\boldsymbol{y})\big) - \lim_{t\to 0^-} \boldsymbol{f}\big(\boldsymbol{y} + t\boldsymbol{n}(\boldsymbol{y})\big).$$

For composite materials, the cell problem (2.7) is augmented with the two transmission conditions on the interface $\partial\omega$

$$\big[\boldsymbol{w}_{ij}(\boldsymbol{y})\big] = \boldsymbol{0} \quad \text{and} \quad \big[\boldsymbol{A}(\boldsymbol{y}) : \nabla \boldsymbol{w}_{ij}(\boldsymbol{y})\big]\,\boldsymbol{n}(\boldsymbol{y}) = \boldsymbol{0} \quad \text{for } \boldsymbol{y} \in \partial\omega. \tag{2.10}$$

With these conditions, the variational formulation of the cell problem (2.7) for $\boldsymbol{v} \in [H^1_{\mathrm{per}}(Y)]^n$ becomes

$$\int_Y \big(\boldsymbol{A}(\boldsymbol{y}) : (e_{ij} + \nabla \boldsymbol{w}_{ij})\big) : \nabla \boldsymbol{v}\,\mathrm{d}\boldsymbol{y} = \boldsymbol{0}. \tag{2.11}$$

Formula (2.11) together with (2.8) shows the dependency of the homogenized elasticity tensor $\boldsymbol{A}^*(\omega)$ on the choice of the interface ω. Also, $\boldsymbol{A}^*(\omega)$ inherits from the elasticity tensor $\boldsymbol{A}(\boldsymbol{y})$ the symmetry properties and the uniform ellipticity. Therefore, the homogenized system on Ω, written in the form

$$\begin{cases} -\operatorname{div}\big(\boldsymbol{\sigma}^*(\omega, \boldsymbol{u})\big) = \boldsymbol{f}, & \text{in } \Omega, \\ \boldsymbol{u} = \boldsymbol{0}, & \text{on } \Gamma_D, \\ \boldsymbol{\sigma}^*\big(\omega, \boldsymbol{u})\big)\boldsymbol{n} = \boldsymbol{g}, & \text{on } \Gamma_N, \\ \boldsymbol{\sigma}^*\big(\omega, \boldsymbol{u})\big)\boldsymbol{n} = \boldsymbol{0}, & \text{on } \Gamma = \partial\Omega \setminus (\Gamma_D \cup \Gamma_N), \end{cases}$$

with the (effective) Cauchy stress tensor is $\boldsymbol{\sigma}^*(\omega, \boldsymbol{u}) \coloneqq \boldsymbol{A}^*(\omega) : \nabla \boldsymbol{u}$, has a unique solution for all sufficiently smooth subsets ω.

2.4. **Goal of optimization.** In this article, we ask for the shape $\omega \subset Y$, such that the least squares mismatch

$$J(\omega) \coloneqq \frac{1}{2}\|\boldsymbol{B} - \boldsymbol{A}^*(\omega)\|_F^2 = \frac{1}{2}\sum_{i,j,k,l=1}^{n} \Big(b_{ijkl} - a^*_{ijkl}(\omega)\Big)^2 \tag{2.13}$$

between the effective tensor $\boldsymbol{A}^*(\omega)$ and a desired elasticity tensor $\boldsymbol{B} \in \mathbb{R}^{n^4}$ with coefficients b_{ijkl} is minimized with respect to the Frobenius norm $\|\cdot\|_F$. In order to solve this problem by a gradient based optimization method, we shall compute the shape derivative of $J(\omega)$. We begin by finding an expression for the shape derivative of the coefficients of the effective tensor $\boldsymbol{A}^*(\omega)$.

3. Shape derivative of the effective tensor

3.1. **Local shape derivative.** We introduce a vector field $\boldsymbol{h} : Y \to Y$ that vanishes on the boundary ∂Y and consider the perturbation of identity operator $T_t \coloneqq \boldsymbol{I} + t\boldsymbol{h}$. T_t is a diffeomorphism for t small enough, which preserves Y. We define the function

$$\boldsymbol{\phi}_{ij}(\boldsymbol{y}) \coloneqq \boldsymbol{w}_{ij}(\boldsymbol{y}) + \boldsymbol{y}_{ij} \quad \text{for } i,j = 1,\dots,n,$$

where $\boldsymbol{w}_{ij}$ is the unique solution of the cell problem (2.7) and $\boldsymbol{y}_{ij}$ is a column vector with entries 0 except in the i-th row the entry y_j. Then, $\nabla \boldsymbol{y}_{ij} = e_{ij}$ and the cell problem (2.7) becomes

$$\operatorname{div}(\boldsymbol{A} : \nabla \boldsymbol{\phi}_{ij}) = \boldsymbol{0} \quad \text{for } i,j = 1,\dots,n. \tag{3.1}$$

We define the normal component of the gradient of a function $\boldsymbol{v} \in [H^1_{\mathrm{per}}(Y)]^n$ as

$$\nabla_{\boldsymbol{n}} \boldsymbol{v} \coloneqq \boldsymbol{n}\boldsymbol{n}^{\intercal} \nabla \boldsymbol{v} = \boldsymbol{n}(\partial_{\boldsymbol{n}} \boldsymbol{v})^{\intercal}.$$

Moreover, it follows that the jump of the function $\boldsymbol{v}$ through $\partial\omega$ satisfies

$$[\nabla \boldsymbol{v}] = [\nabla_{\boldsymbol{n}} \boldsymbol{v}]\,. \tag{3.2}$$

We present next the following theorem, which specifies the system of equations the local shape derivative $\delta\boldsymbol{\phi}_{ij}$ satisfies on Y. As the local shape derivative has a jump at $\partial\omega$, we introduce the broken H^1-space in accordance with

$$\mathcal{X} \coloneqq \big\{ f \in L^2(Y) : f|_{Y\setminus\overline{\omega}} \in H^1_{\mathrm{per}}(Y \setminus \overline{\omega}) \text{ and } f|_{\omega} \in H^1(\omega) \big\}.$$

Theorem 2 (Shape derivative of the cell problem)**.** The shape derivative $\delta\boldsymbol{\phi}_{ij}$ in $\mathcal{X}$ of the function $\boldsymbol{\phi}_{ij} = \boldsymbol{w}_{ij} + \boldsymbol{y}_{ij}$ is the solution in Y of the transmission problem

$$\operatorname{div}\Big(\boldsymbol{A} : \nabla \delta\boldsymbol{\phi}_{ij}\Big) = \boldsymbol{0} \qquad \text{in } \omega \cup Y \setminus \overline{\omega}, \tag{3.3a}$$

$$[\delta\boldsymbol{\phi}_{ij}] = -\langle \boldsymbol{h}, \boldsymbol{n}\rangle \Big[\partial_{\boldsymbol{n}} \boldsymbol{\phi}_{ij}\Big] \qquad \text{on } \partial\omega, \tag{3.3b}$$

$$\Big[\Big(\boldsymbol{A} : \nabla \delta\boldsymbol{\phi}_{ij}\Big)\,\boldsymbol{n}\Big] = \Big[\operatorname{div}_{\boldsymbol{\tau}}\Big(\langle \boldsymbol{h}, \boldsymbol{n}\rangle \Big(\boldsymbol{A}(\boldsymbol{y}) : \nabla \boldsymbol{\phi}_{ij}\Big)\Big)\Big] \qquad \text{on } \partial\omega. \tag{3.3c}$$

Here, $\nabla_{\boldsymbol{\tau}} \boldsymbol{\phi}_{ij} \coloneqq \nabla \boldsymbol{\phi}_{ij} - \nabla_{\boldsymbol{n}} \boldsymbol{\phi}_{ij} = (\boldsymbol{I} - \boldsymbol{n}\boldsymbol{n}^{\intercal}) \nabla \boldsymbol{\phi}_{ij}$ is the surface gradient of the function $\boldsymbol{\phi}_{ij}$ and, given a matrix function $B = (b_1, \dots, b_n)^{\intercal} \in C^1(\partial\omega, \mathbb{R}^{n\times n})$, the surface divergence is $\operatorname{div}_{\boldsymbol{\tau}}(B) \coloneqq \big(\operatorname{tr}(\nabla_{\boldsymbol{\tau}} b_1), \dots, \operatorname{tr}(\nabla_{\boldsymbol{\tau}} b_n)\big)^{\intercal}$.

Proof. The proof is carried out in the usual way, compare [6]. We prove the material derivative exists, then characterize it, and finally express the shape derivative.

1. Computation of the material derivative. Let $\boldsymbol{\phi}^t_{ij}(\boldsymbol{y})$ be the unique solution of the cell problem (2.7) on the perturbed domain $Y_t \coloneqq \{y + t\boldsymbol{h}(\boldsymbol{y}) \big| y \in Y\}$ and set

$$\boldsymbol{A}_t(\boldsymbol{y}) \coloneqq \boldsymbol{A}_1\big(T_t(\boldsymbol{y})\big) + \Big(\boldsymbol{A}_2\left(T_t(\boldsymbol{y})\right) - \boldsymbol{A}_1\big(T_t(\boldsymbol{y})\big)\Big)\mathbb{1}_{\omega}(\boldsymbol{y}).$$

Then, the transported function $\tilde{\boldsymbol{\phi}}_{ij}(t,\boldsymbol{y}) \coloneqq \boldsymbol{\phi}_{ij}^t\big(T_t(\boldsymbol{y})\big)$, satisfies the variational equation

$$\begin{aligned}\int_Y \Big(\boldsymbol{A}_t(\boldsymbol{y}) : \Big(\big(\nabla T_t(\boldsymbol{y})\big)^{-1} \nabla \tilde{\boldsymbol{\phi}}_{ij}(t,\boldsymbol{y}) \Big) \Big) \\ : \Big(\big(\nabla T_t(\boldsymbol{y})\big)^{-1} \nabla \boldsymbol{v}(\boldsymbol{y}) \Big) \det\big(\mathrm{D}T_t(\boldsymbol{y})\big)\,\mathrm{d}\boldsymbol{y} = 0\end{aligned} \tag{3.4}$$

for all $\boldsymbol{v} \in [H^1_{\mathrm{per}}(Y)]^n$. Using the property $A : (BC) = (B^\intercal A) : C$ of the Frobenius product for square matrices A, B, C and subtracting the equation (2.11) from the equation (3.4) above, we find for any $t > 0$

$$\begin{aligned}\int_Y \Big\{ \det\big(\mathrm{D}T_t(\boldsymbol{y})\big) \big(\nabla T_t(\boldsymbol{y})\big)^{-\intercal} \Big(\boldsymbol{A}_t(\boldsymbol{y}) : \Big(\big(\nabla T_t(\boldsymbol{y})\big)^{-1} \nabla \tilde{\boldsymbol{\phi}}_{ij}(t,\boldsymbol{y}) \Big) \Big) \\ - \Big(\boldsymbol{A}(\boldsymbol{y}) : \nabla \boldsymbol{\phi}_{ij}(\boldsymbol{y}) \Big) \Big\} : \nabla \boldsymbol{v}(\boldsymbol{y})\,\mathrm{d}\boldsymbol{y} = 0\end{aligned}$$

for all $\boldsymbol{v} \in [H^1_{\mathrm{per}}(Y)]^n$. Now, to this equation we add and subtract equal terms in order to obtain the equivalent equation

$$\begin{aligned}&\int_Y \Big\{ \Big(\big(\nabla T_t(\boldsymbol{y})\big)^{-\intercal} - \boldsymbol{I} \Big) \Big(\tilde{\boldsymbol{A}}(t,\boldsymbol{y}) : \Big(\big(\nabla T_t(\boldsymbol{y})\big)^{-1} \nabla \tilde{\boldsymbol{\phi}}_{ij}(t,\boldsymbol{y}) \Big) \Big) \\ &\quad + \Big(\tilde{\boldsymbol{A}}(t,y) : \Big(\Big(\big(\nabla T_t(\boldsymbol{y})\big)^{-1} - \boldsymbol{I} \Big) \nabla \tilde{\boldsymbol{\phi}}_{ij}(t,\boldsymbol{y}) \Big) \Big) \\ &\quad + \Big(\det\big(\mathrm{D}T_t(\boldsymbol{y})\big) - 1 \Big) \Big(\boldsymbol{A}\big(T_t(\boldsymbol{y})\big) : \nabla \tilde{\boldsymbol{\phi}}_{ij}(t,\boldsymbol{y}) \Big) \\ &\quad + \Big(\big(\boldsymbol{A}_t(\boldsymbol{y}) - \boldsymbol{A}(\boldsymbol{y})\big) : \nabla \tilde{\boldsymbol{\phi}}_{ij}(t,\boldsymbol{y}) \Big) \Big\} : \nabla \boldsymbol{v}\,\mathrm{d}\boldsymbol{y} \\ &\qquad = - \int_Y \Big(\boldsymbol{A}(\boldsymbol{y}) : \Big(\nabla \tilde{\boldsymbol{\phi}}_{ij}(t,\boldsymbol{y}) - \nabla \boldsymbol{\phi}_{ij}(\boldsymbol{y}) \Big) \Big) : \nabla \boldsymbol{v}\,\mathrm{d}\boldsymbol{y},\end{aligned} \tag{3.5}$$

where $\tilde{\boldsymbol{A}}(t,\boldsymbol{y}) \coloneqq \det\big(\mathrm{D}T_t(\boldsymbol{y})\big) \boldsymbol{A}_t(\boldsymbol{y})$. We replace the test function $\boldsymbol{v}$ by $\tilde{\boldsymbol{\phi}}_{ij}(t,\cdot) - \boldsymbol{\phi}_{ij}$ in (3.5). Then, with the Cauchy-Schwarz inequality, the uniform ellipticity of $\boldsymbol{A}(\boldsymbol{y})$ for all $\boldsymbol{y} \in Y$, and dividing by $t > 0$, we obtain the inequality

$$\begin{aligned}\underline{\alpha} \left\| \frac{\nabla \tilde{\boldsymbol{\phi}}_{ij}(t,\cdot) - \nabla \boldsymbol{\phi}_{ij}}{t} \right\|_{L^2(Y)} &\le \left\| \nabla \tilde{\boldsymbol{\phi}}_{ij}(t,\cdot) \right\|_{L^2(Y)} \Bigg\{ \|\boldsymbol{A}\|_{L^\infty(Y)} \left\| \frac{\det\big(\mathrm{D}T_t(\cdot)\big) - 1}{t} \right\|_{L^\infty(Y)} \\ &\quad + \left\| \frac{\boldsymbol{A}_1\big(T_t(\cdot)\big) - \boldsymbol{A}_1(\cdot)}{t} \right\|_{L^\infty(Y\setminus\overline{\omega})} + \left\| \frac{\boldsymbol{A}_2\big(T_t(\cdot)\big) - \boldsymbol{A}_2(\cdot)}{t} \right\|_{L^\infty(\omega)} \\ &\quad + C(t) \|\boldsymbol{A}\|_{L^\infty(Y)} \left\| \frac{\big(\nabla T_t(\cdot)\big)^{-1} - \boldsymbol{I}}{t} \right\|_{L^\infty(Y)} \Bigg\},\end{aligned}$$

where $C(t) \to 1$ for $t \to 0$ and $\underline{\alpha} = \min_{\boldsymbol{y}\in Y} \alpha_{\boldsymbol{y}}$, cf. (2.5). The four functions $t \mapsto \big(\nabla T_t(\boldsymbol{y})\big)^{-1}$, $t \mapsto \det\big(\mathrm{D}T_t(\boldsymbol{y})\big)$, $t \mapsto \boldsymbol{A}_1\big(T_t(\boldsymbol{y})\big)$ and $t \mapsto \boldsymbol{A}_2\big(T_t(\boldsymbol{y})\big)$ are differentiable

at each $\boldsymbol{y} \in Y$. Thus, the term on the right-hand side is bounded for $t \to 0$. Therefore, the fraction $\big(\tilde{\boldsymbol{\phi}}_{ij}(t,\cdot) - \boldsymbol{\phi}_{ij}\big)/t$ is bounded in $[H^1_{\mathrm{per}}(Y)]^n$, it is weakly convergent in $[H^1_{\mathrm{per}}(Y)]^n$, and its weak limit is the material derivative $\dot{\boldsymbol{\phi}}_{ij} \in [H^1_{\mathrm{per}}(Y)]^n$.

We divide (3.5) by t and compute $t \to 0$ to obtain the equation which is satisfied by the material derivative $\dot{\boldsymbol{\phi}}_{ij}$:

$$
\begin{aligned}
-\int_Y \Big(\boldsymbol{A}(\boldsymbol{y}) : \nabla\dot{\boldsymbol{\phi}}_{ij}\Big) : \nabla\boldsymbol{v}\,\mathrm{d}\boldsymbol{y} &= \int_Y \Big\{ (\nabla\boldsymbol{h}) \intercal \Big(\boldsymbol{A}(\boldsymbol{y}) : \nabla\boldsymbol{\phi}_{ij}\Big) \\
&\quad + \Big(\boldsymbol{A}(\boldsymbol{y}) : \Big(\nabla\boldsymbol{h}\nabla\boldsymbol{\phi}_{ij}\Big)\Big) + \operatorname{div}(\boldsymbol{h})\Big(\boldsymbol{A}(\boldsymbol{y}) : \nabla\boldsymbol{\phi}_{ij}\Big)\Big\} : \nabla\boldsymbol{v}\,\mathrm{d}\boldsymbol{y} \\
&\quad + \int_{Y\setminus\overline{\omega}} \Big(\big(\boldsymbol{h}(\nabla\otimes\boldsymbol{A}_1)\big) : \nabla\boldsymbol{\phi}_{ij}\Big) : \nabla\boldsymbol{v}\,\mathrm{d}\boldsymbol{y} + \int_{\omega} \Big(\big(\boldsymbol{h}(\nabla\otimes\boldsymbol{A}_2)\big) : \nabla\boldsymbol{\phi}_{ij}\Big) : \nabla\boldsymbol{v}\,\mathrm{d}\boldsymbol{y}.
\end{aligned} \tag{3.6}
$$

In this equation, for $m = 1, 2$, $\big(\boldsymbol{h}(\nabla\otimes\boldsymbol{A}_m)\big)$ denotes the fourth order tensor with entries $\langle \boldsymbol{h}(\boldsymbol{y}), \nabla a^m_{ijkl}(\boldsymbol{y})\rangle$, where a^m_{ijkl} are the entries of $\boldsymbol{A}_m(\boldsymbol{y})$.

2. Strong convergence to the material derivative. In order to prove strong convergence of $\big(\tilde{\boldsymbol{\phi}}_{ij}(t,\cdot) - \boldsymbol{\phi}_{ij}\big)/t$ to $\dot{\boldsymbol{\phi}}_{ij} \in [H^1_{\mathrm{per}}(Y)]^n$, we use $\big(\tilde{\boldsymbol{\phi}}_{ij}(t,\cdot) - \boldsymbol{\phi}_{ij}\big)/t$ as test function in (3.5) and divide the equation by $t > 0$, which yields

$$
\begin{aligned}
-\int_Y \big(\boldsymbol{A}(\boldsymbol{y}) : N_1(t,\boldsymbol{y})\big) : N_1(t,\boldsymbol{y})\,\mathrm{d}\boldsymbol{y} &= \int_Y \Bigg\{ \left(\tilde{\boldsymbol{A}}(t,\boldsymbol{y}) : \left(\frac{\big(\nabla T_t(\boldsymbol{y})\big)^{-1} - \boldsymbol{I}}{t} \right) N_2(t,\boldsymbol{y}) \right) \\
&\quad + \frac{\det\big(\mathrm{D}T_t(\boldsymbol{y})\big) - 1}{t} \big(\boldsymbol{A}_t(\boldsymbol{y}) : N_2(t,\boldsymbol{y})\big) \Bigg\} : N_1(t,\boldsymbol{y})\,\mathrm{d}\boldsymbol{y} \\
&\quad + \int_Y \left(\tilde{\boldsymbol{A}}(t,\boldsymbol{y}) : \Big(\big(\nabla T_t(\boldsymbol{y})\big)^{-1}\Big) N_2(t,\boldsymbol{y}) \right) : \left(\frac{\big(\nabla T_t(\boldsymbol{y})\big)^{-1} - \boldsymbol{I}}{t} N_1(t,\boldsymbol{y}) \right) \mathrm{d}\boldsymbol{y} \\
&\quad + \int_{Y\setminus\overline{\omega}} \left(\frac{\boldsymbol{A}_1\big(T_t(\boldsymbol{y})\big) - \boldsymbol{A}_1(\boldsymbol{y})}{t} : N_2(t,\boldsymbol{y}) \right) : N_1(t,\boldsymbol{y})\,\mathrm{d}\boldsymbol{y} \\
&\quad + \int_{\omega} \left(\frac{\boldsymbol{A}_2\big(T_t(\boldsymbol{y})\big) - \boldsymbol{A}_2(\boldsymbol{y})}{t} : N_2(t,\boldsymbol{y}) \right) : N_1(t,\boldsymbol{y})\,\mathrm{d}\boldsymbol{y},
\end{aligned}
$$

where $N_1(t,\boldsymbol{y}) \coloneqq \nabla\big(\tilde{\boldsymbol{\phi}}_{ij}(t,\boldsymbol{y}) - \boldsymbol{\phi}_{ij}(\boldsymbol{y})\big)/t$ and $N_2(t,\boldsymbol{y}) \coloneqq N_1(t,\boldsymbol{y}) \cdot t + \nabla\boldsymbol{\phi}_{ij}(\boldsymbol{y})$. Now, considering $t \to 0$ in the equation above, with the weak convergence of $N_1(t,\boldsymbol{y})$ to the material derivative $\dot{\boldsymbol{\phi}}_{ij}$ and (3.6), we conclude that

$$
\int_Y \big(\boldsymbol{A}(\boldsymbol{y}) : N_1(t,\boldsymbol{y})\big) : N_1(t,\boldsymbol{y})\,\mathrm{d}\boldsymbol{y} \quad \longrightarrow \quad \int_Y \Big(\boldsymbol{A}(\boldsymbol{y}) : \nabla\dot{\boldsymbol{\phi}}_{ij}\Big) : \nabla\dot{\boldsymbol{\phi}}_{ij}\,\mathrm{d}\boldsymbol{y}
$$

and therefore that $N_1(t,\cdot)$ converges strongly in $[L^2(Y)]^n$. Poincaré's inequality then implies that $\big(\tilde{\boldsymbol{\phi}}_{ij}(t,\cdot) - \boldsymbol{\phi}_{ij}(t)\big)/t$ converges strongly in $[H^1_{\mathrm{per}}(Y)]^n$ to the material derivative $\dot{\boldsymbol{\phi}}_{ij}$.

With the computations above, the material derivative exists and satisfies the variational problem: find $\dot{\boldsymbol{\phi}}_{ij} \in [H^1_{\mathrm{per}}(Y)]^n$ such that

$$\begin{aligned}\int_Y \left(\boldsymbol{A} : \nabla \dot{\boldsymbol{\phi}}_{ij}\right) : \nabla \boldsymbol{v} \,\mathrm{d}\boldsymbol{y} = \int_Y \Big\{ (\nabla \boldsymbol{h})^{\intercal} \left(\boldsymbol{A} : \nabla \boldsymbol{\phi}_{ij}\right) + \boldsymbol{A} : \left(\mathrm{D}\boldsymbol{\phi}_{ij}\mathrm{D}\boldsymbol{h}\right) \\ - \operatorname{div}(\boldsymbol{h}) \left(\boldsymbol{A} : \nabla \boldsymbol{\phi}_{ij}\right) \Big\} : \nabla \boldsymbol{v} \,\mathrm{d}\boldsymbol{y} - \int_{Y\setminus\overline{\omega}} \left(\left(\boldsymbol{h}(\nabla \otimes \boldsymbol{A}_1)\right) : \nabla \boldsymbol{\phi}_{ij}\right) : \nabla \boldsymbol{v} \,\mathrm{d}\boldsymbol{y} \\ - \int_{\omega} \left(\left(\boldsymbol{h}(\nabla \otimes \boldsymbol{A}_2)\right) : \nabla \boldsymbol{\phi}_{ij}\right) : \nabla \boldsymbol{v} \,\mathrm{d}\boldsymbol{y}.\end{aligned} \tag{3.7}$$

3. Recovering the shape derivative. Employing integration by parts in (3.7), we can rewrite the weak problem solved by the material derivative as

$$\begin{aligned}\int_Y \left(\boldsymbol{A} : \nabla \dot{\boldsymbol{\phi}}_{ij}\right) : \nabla \boldsymbol{v} \,\mathrm{d}\boldsymbol{y} = \int_{\partial\omega} \left[\left\langle \left(\boldsymbol{A} : \nabla \boldsymbol{\phi}_{ij}\right) \boldsymbol{n}, \mathrm{D}\boldsymbol{v}\boldsymbol{h} \right\rangle\right] - \left[\langle \boldsymbol{h}, \boldsymbol{n}\rangle \left(\boldsymbol{A} : \nabla \boldsymbol{\phi}_{ij}\right) : \nabla \boldsymbol{v}\right] \mathrm{d}o \\ + \int_{Y\setminus\overline{\omega}} \left(\boldsymbol{A}_1 : \nabla \left(\mathrm{D}\boldsymbol{\phi}_{ij}\boldsymbol{h}\right)\right) : \nabla \boldsymbol{v} \,\mathrm{d}\boldsymbol{y} + \int_{\omega} \left(\boldsymbol{A}_2 : \nabla \left(\mathrm{D}\boldsymbol{\phi}_{ij}\boldsymbol{h}\right)\right) : \nabla \boldsymbol{v} \,\mathrm{d}\boldsymbol{y}.\end{aligned}$$

From [7], we have the relation $\dot{\boldsymbol{\phi}}_{ij} = \delta\boldsymbol{\phi}_{ij} + \mathrm{D}\boldsymbol{\phi}_{ij}\boldsymbol{h}$ between the shape derivative and the material derivative. Thus, we can replace the material derivative in (3.7) by the shape derivative to arrive at

$$\begin{aligned}\int_{Y\setminus\overline{\omega}} \left(\boldsymbol{A}_1 : \nabla \delta\boldsymbol{\phi}_{ij}\right) : \nabla \boldsymbol{v} \,\mathrm{d}\boldsymbol{y} + \int_{\omega} \left(\boldsymbol{A}_2 : \nabla \delta\boldsymbol{\phi}_{ij}\right) : \nabla \boldsymbol{v} \,\mathrm{d}\boldsymbol{y} \\ = - \int_{\partial\omega} \left[\langle \boldsymbol{h}, \boldsymbol{n}\rangle \left(\boldsymbol{A} : \nabla \boldsymbol{\phi}_{ij}\right) : \nabla \boldsymbol{v}\right] - \left[\left\langle \left(\boldsymbol{A} : \nabla \boldsymbol{\phi}_{ij}\right) \boldsymbol{n}, \mathrm{D}\boldsymbol{v}\boldsymbol{h} \right\rangle\right] \mathrm{d}o.\end{aligned} \tag{3.8}$$

Since $\dot{\boldsymbol{\phi}}_{ij}$ has no jump at $\partial\omega$ as a function in $[H^1_{\mathrm{per}}(Y)]^n$, we conclude the first transmission condition for $\delta\boldsymbol{\phi}_{ij}$ at the interface $\partial\omega$:

$$[\delta\boldsymbol{\phi}_{ij}] = -[\mathrm{D}\boldsymbol{\phi}_{ij}\boldsymbol{h}] = - \left[\langle \boldsymbol{h}, \boldsymbol{n}\rangle \partial_{\boldsymbol{n}} \boldsymbol{\phi}_{ij}\right].$$

Next, with (2.10), (3.2), and the symmetry of the matrix $\boldsymbol{A} : \nabla\boldsymbol{\phi}_{ij}$, we rewrite (3.8) as

$$\begin{aligned}\int_{Y\setminus\overline{\omega}} \left(\boldsymbol{A}_1 : \nabla \delta\boldsymbol{\phi}_{ij}\right) : \nabla \boldsymbol{v} \,\mathrm{d}\boldsymbol{y} + \int_{\omega} \left(\boldsymbol{A}_2 : \nabla \delta\boldsymbol{\phi}_{ij}\right) : \nabla \boldsymbol{v} \,\mathrm{d}\boldsymbol{y} \\ = - \int_{\partial\omega} \left[\langle \boldsymbol{h}, \boldsymbol{n}\rangle \left(\boldsymbol{A} : \nabla \boldsymbol{\phi}_{ij}\right) : \nabla_{\boldsymbol{\tau}} \boldsymbol{v}\right] \mathrm{d}o.\end{aligned} \tag{3.9}$$

We proceed with integration by parts over ω and $Y \setminus \overline{\omega}$ on the left-hand side and with integration by parts over the closed surface $\partial\omega$ on the right-hand side of the equation. By

using (2.10) again, this yields

$$\int_{Y\setminus\overline{\omega}} \left\langle \operatorname{div}\left(\boldsymbol{A}_1 : \nabla\delta\boldsymbol{\phi}_{ij})\right), \boldsymbol{v}\right\rangle \mathrm{d}\boldsymbol{y} + \int_{\omega} \left\langle \operatorname{div}\left(\boldsymbol{A}_2 : \nabla\delta\boldsymbol{\phi}_{ij})\right), \boldsymbol{v}\right\rangle \mathrm{d}\boldsymbol{y} - \int_{\partial\omega} \left[\left\langle \left(\boldsymbol{A} : \nabla\delta\boldsymbol{\phi}_{ij}\right)\boldsymbol{n}, \boldsymbol{v}\right\rangle\right] \mathrm{d}o = -\int_{\partial\omega} \left[\left\langle \operatorname{div}_{\boldsymbol{\tau}}\left(\langle \boldsymbol{h}, \boldsymbol{n}\rangle \left(\boldsymbol{A} : \nabla\boldsymbol{\phi}_{ij}\right)\right), \boldsymbol{v}\right\rangle\right] \mathrm{d}o.$$

We deduce that $\delta\boldsymbol{\phi}_{ij}$ is harmonic in both subdomains ω and $Y\setminus\overline{\omega}$, while the second transmission condition is also deduced from this equation. □

3.2. **Sensitivity of the effective tensor.** From [7, 24], given a function $f : \mathbb{R}\times\mathbb{R}^n \to \mathbb{R}$, we have

$$\left(\frac{\mathrm{d}}{\mathrm{d}t}\int_{T_t(\boldsymbol{y})} f(t,y)\,\mathrm{d}\boldsymbol{y}\right)_{|t=0} = \int_Y \frac{\mathrm{d}}{\mathrm{d}t} f(t,\boldsymbol{y}) + \operatorname{div}\left(f(0,\boldsymbol{y})\boldsymbol{h}\right)\mathrm{d}\boldsymbol{y}. \tag{3.10}$$

This formula appears in the literature in Hadamard's shape calculus and also as the Reynolds transport theorem in continuum mechanics.

Theorem 3 (Shape derivative of the coefficients of the effective tensor)**.** The shape derivatives of the entries a^*_{ijkl} of the effective tensor given by (2.8) are

$$\delta a^*_{iklj}(\omega)[\boldsymbol{h}] = -\int_{\partial\omega} \langle \boldsymbol{h}, \boldsymbol{n}\rangle \left\{ \left[\boldsymbol{A}(\boldsymbol{y}) : \nabla\boldsymbol{\phi}_{kl}\right] : \nabla_{\boldsymbol{\tau}}\boldsymbol{\phi}_{ij} - \left\langle \left(\boldsymbol{A}_2(\boldsymbol{y}) : \nabla\boldsymbol{\phi}^-_{ij}\right)\boldsymbol{n}, \left[\mathrm{D}\boldsymbol{\phi}_{kl}\right]\boldsymbol{n}\right\rangle \right\} \mathrm{d}o,$$

where $\boldsymbol{\phi}_{ij}(\boldsymbol{y}) = \boldsymbol{w}_{ij}(\boldsymbol{y}) + \boldsymbol{y}_{ij}$ with $\boldsymbol{w}_{ij} \in [H^1_{\mathrm{per}}(Y)]^n$ are the unique solutions of the cell problem (2.7) for all $i,j = 1,\dots,n$.

Proof. We set $f(t,\boldsymbol{y}) = \left(\boldsymbol{A}(\boldsymbol{y}) : \nabla\boldsymbol{\phi}^t_{ij}(\boldsymbol{y})\right) : \nabla\boldsymbol{\phi}^t_{kl}(\boldsymbol{y})$. Since the value of the function $\delta\boldsymbol{\phi}_{ij}$ has a jump through $\partial\omega$, we want to consider $\nabla\delta\boldsymbol{\phi}_{ij}$ inside and outside the interface separately. Therefore, we introduce the set Θ, which may designate either the set $Y\setminus\overline{\omega}$ or ω. Then, for the first term in Hadamard's formula (3.10), we find

$$\int_\Theta \frac{\mathrm{d}}{\mathrm{d}t} f(t,\boldsymbol{y})\,\mathrm{d}\boldsymbol{y} = \int_\Theta \left(\boldsymbol{A}(\boldsymbol{y}) : \nabla\delta\boldsymbol{\phi}_{ij}\right) : \nabla\boldsymbol{\phi}_{kl} + \left(\boldsymbol{A}(\boldsymbol{y}) : \nabla\boldsymbol{\phi}_{ij}\right) : \nabla\delta\boldsymbol{\phi}_{kl}\,\mathrm{d}\boldsymbol{y}.$$

Hence, we arrive at

$$\int_Y \frac{\mathrm{d}}{\mathrm{d}t} f(t,\boldsymbol{y})\,\mathrm{d}\boldsymbol{y} = -\int_{\partial\omega} \langle \boldsymbol{h}, \boldsymbol{n}\rangle \left\{ \left[\boldsymbol{A}(\boldsymbol{y}) : \nabla\boldsymbol{\phi}_{ij}\right] : \nabla_{\boldsymbol{\tau}}\boldsymbol{\phi}_{kl} + \left[\boldsymbol{A}(\boldsymbol{y}) : \nabla\boldsymbol{\phi}_{kl}\right] : \nabla_{\boldsymbol{\tau}}\boldsymbol{\phi}_{ij} \right\} \mathrm{d}o,$$

where we added the equation with $\Theta = Y\setminus\overline{\omega}$ to the one with $\Theta = \omega$ and used the results from Theorem 2.

For the second term in Hadamard's formula (3.10) with the divergence theorem, we compute

$$\int_Y \operatorname{div}\big(f(0,\boldsymbol{y})\boldsymbol{h}\big)\,\mathrm{d}\boldsymbol{y} = \int_{\partial\omega}\big[f(0,\boldsymbol{y})\langle\boldsymbol{h},\boldsymbol{n}\rangle\big]\,\mathrm{d}o = \int_{\partial\omega}\Big[\langle\boldsymbol{h},\boldsymbol{n}\rangle\Big(\boldsymbol{A}(\boldsymbol{y}):\nabla\boldsymbol{\phi}_{ij}\Big):\nabla\boldsymbol{\phi}_{kl}\Big]\,\mathrm{d}o$$
$$= \int_{\partial\omega}\left\{\Big[\boldsymbol{A}(\boldsymbol{y}):\nabla\boldsymbol{\phi}_{ij}\Big]:\nabla_{\boldsymbol{\tau}}\boldsymbol{\phi}_{kl} + \Big\langle\Big(\boldsymbol{A}_2(\boldsymbol{y}):\nabla\boldsymbol{\phi}_{ij}^-\Big)\boldsymbol{n}, [\mathrm{D}\boldsymbol{\phi}_{kl}]\,\boldsymbol{n}\Big\rangle\right\}\langle\boldsymbol{h},\boldsymbol{n}\rangle\,\mathrm{d}o.$$

Putting the two terms together yields the desired result of the lemma. □

Remark 4. By substituting back $\boldsymbol{\phi}_{ij} = \boldsymbol{w}_{ij} + \boldsymbol{y}_{ij}$, we arrive at the computable expression

$$\begin{aligned}\delta a^*_{iklj}(\omega)[\boldsymbol{h}] = -\int_{\partial\omega}\langle\boldsymbol{h},\boldsymbol{n}\rangle\Big\{&\big[\boldsymbol{A}(\boldsymbol{y}):\nabla(\boldsymbol{w}_{kl}+y_{kl})\big]:\nabla_{\boldsymbol{\tau}}(\boldsymbol{w}_{ij}+\boldsymbol{y}_{ij})\\ &-\Big\langle\Big(\boldsymbol{A}_2(\boldsymbol{y}):(\nabla\boldsymbol{w}_{ij}^- + \boldsymbol{y}_{ij})\Big)\boldsymbol{n}, \Big(\mathrm{D}\boldsymbol{w}_{kl}^+ - \mathrm{D}\boldsymbol{w}_{kl}^-\Big)\boldsymbol{n}\Big\rangle\Big\}\,\mathrm{d}o,\end{aligned} \tag{3.11}$$

where $n_{ij} = e_{ij}\boldsymbol{n}$ denotes the vector with the i-th component of $\boldsymbol{n}$ at the j-th position and the j-th component of $\boldsymbol{n}$ at the i-th position.

The homogenized elastic tensor $\boldsymbol{A}^*$ satisfies $\boldsymbol{A}^* = (\boldsymbol{A}^*)^\intercal$. With numerical inaccuracies in the implementation, the symmetry properties of the tensor get lost. Thus, we compute the mean $(\delta a^*_{iklj} + \delta a^*_{kijl})/2$ instead.

3.3. **Shape derivative of the least square matching.** With the help of Theorem 3 and the chain rule

$$\delta J(\omega)[\boldsymbol{h}] = \sum_{i,j,k,l=1}^{n}\Big(a^*_{ijkl}(\omega) - b_{ijkl}\Big)\,\delta a^*_{ijkl}(\omega)[\boldsymbol{h}],$$

we can easily determine the shape derivative of the objective $J(\omega)$ given by (2.13).

Proposition 5. The shape derivative of the objective function from (2.13) reads

$$\begin{aligned}\delta J(\omega)[\boldsymbol{h}] = \sum_{i,j,k,l=1}^{n}\Big(b_{ijkl} - a^*_{ijkl}(\omega)\Big)\int_{\partial\omega}\langle\boldsymbol{h},\boldsymbol{n}\rangle\Big\{&\big[\boldsymbol{A}(\boldsymbol{y}):\nabla\boldsymbol{\phi}_{kl}\big]:\nabla_{\boldsymbol{\tau}}\boldsymbol{\phi}_{ij}\\ &-\Big\langle\Big(\boldsymbol{A}_2(\boldsymbol{y}):\nabla\boldsymbol{\phi}_{ij}^-\Big)\boldsymbol{n}, [\mathrm{D}\boldsymbol{\phi}_{kl}]\,\boldsymbol{n}\Big\rangle\Big\}\,\mathrm{d}o.\end{aligned} \tag{3.12}$$

3.4. **Perforated plates and scaffold structures.** We consider now the n-dimensional unit cube $Y = [0,1]^n$ with a hole ω such that $\omega \Subset Y$. This corresponds to the limiting case $\boldsymbol{A}_2 \to \boldsymbol{0}$ in (2.9) for a composite material. In two spatial dimensions, we get perforated plates, while in three spatial dimensions, we get scaffold structures.

The previous results remain similar when considering $Y \setminus \overline{\omega}$ instead of Y. This means that the cell problem becomes: seek $\boldsymbol{w}_{ij} \in [H^1_{\mathrm{per}}(Y\setminus\overline{\omega})]^n$ with $(\boldsymbol{w}_{ij}, \mathbb{1})_{[L^2(Y\setminus\overline{\omega})]^n}$ such that

$$\begin{aligned}\operatorname{div}\big(\boldsymbol{A}:(e_{ij}+\nabla\boldsymbol{w}_{ij})\big) &= \boldsymbol{0} && \text{in } Y\setminus\overline{\omega},\\ \big(\boldsymbol{A}:\nabla\boldsymbol{w}_{ij}\big)\,\boldsymbol{n} &= -\big(\boldsymbol{A}:e_{ij}\big)\,\boldsymbol{n} && \text{on } \partial\omega.\end{aligned}$$

The homogenized equation in the present situation is

$$-\operatorname{div}\left(\boldsymbol{A}^*(\omega):\nabla\boldsymbol{u}(\boldsymbol{x})\right)=(1-|\omega|)\boldsymbol{f}(\boldsymbol{x}),$$

while the coefficients of the effective tensor are

$$a^*_{ijkl}(\omega)=\int_{Y\setminus\overline{\omega}}\Big(\boldsymbol{A}(\boldsymbol{y}):\big(e_{il}+\nabla\boldsymbol{w}_{il}(\boldsymbol{y})\big)\Big):\big(e_{jk}+\nabla\boldsymbol{w}_{jk}(\boldsymbol{y})\big)\,\mathrm{d}\boldsymbol{y}.$$

Moreover, the system for the shape derivative reads

$$\begin{aligned}
\operatorname{div}\Big(\boldsymbol{A}:\nabla\delta\boldsymbol{\phi}_{ij}\Big)&=\boldsymbol{0} && \text{in } Y\setminus\overline{\omega},\\
\delta\boldsymbol{\phi}_{ij}&=-\langle\boldsymbol{h},\boldsymbol{n}\rangle\partial_{\boldsymbol{n}}\boldsymbol{\phi}_{ij} && \text{on } \partial\omega,\\
\Big(\boldsymbol{A}:\nabla\delta\boldsymbol{\phi}_{ij}\Big)\boldsymbol{n}&=\operatorname{div}_{\boldsymbol{\tau}}\left(\langle\boldsymbol{h},\boldsymbol{n}\rangle\left(\boldsymbol{A}(\boldsymbol{y}):\nabla\boldsymbol{\phi}_{ij}\right)\right) && \text{on } \partial\omega.
\end{aligned}$$

This implies that the shape derivative of the coefficients of the homogenized tensor is given by

$$\delta a^*_{iklj}(\omega)[\boldsymbol{h}]=-\int_{\partial\omega}\langle\boldsymbol{h},\boldsymbol{n}\rangle\left(\boldsymbol{A}(\boldsymbol{y}):\nabla\boldsymbol{\phi}_{ij}\right):\nabla\boldsymbol{\phi}_{kl}\,\mathrm{d}o.$$

Consequently, the shape derivative of the objective function from (2.13) reads

$$\delta J(\omega)[\boldsymbol{h}]=\sum_{i,j,k,l=1}^{n}\Big(b_{ijkl}-a^*_{ijkl}(\omega)\Big)\int_{\partial\omega}\langle\boldsymbol{h},\boldsymbol{n}\rangle\left(\boldsymbol{A}(\boldsymbol{y}):\nabla\boldsymbol{\phi}_{ij}\right):\nabla\boldsymbol{\phi}_{kl}\,\mathrm{d}o. \tag{3.14}$$

4. Implementation and verification

4.1. **Implementation using parametric finite elements.** Our implementation is for the two-dimensional case, i.e. $n=2$. We assume that the sought domain ω is starlike with respect to the midpoint of the unit cell. The boundary $\partial\omega$ of the interface is represented in polar coordinates by the function

$$\gamma(\phi)\coloneqq r(\phi)\begin{pmatrix}\cos(\phi)\\ \sin(\phi)\end{pmatrix},\qquad\text{for } \phi\in[0,2\pi)\,, \tag{4.1}$$

where the radial function $r(\phi)$ is given by the finite Fourier series

$$r(\phi)\coloneqq a_0+\sum_{k=1}^{N}\big\{a_k\cos(k\phi)+a_{-k}\sin(k\phi)\big\}\,, \tag{4.2}$$

where $N\in\mathbb{N}$ and $(a_{-N},\dots,a_0,\dots,a_N)\in\mathbb{R}^{2N+1}$.

The domain $Y=[0,1]\times[0,1]$ is discretized by parametric finite elements with a macro triangulation which is composed of 8 triangles and 8 squares in order to resolve the interface $\partial\omega$ exactly. Each of these elements is transformed from a reference geometry by the help of a diffeomorphism into Y. The squares are interpolated by Coons patches and the triangles with the Zenisek's formula from [28]. The mesh on the reference triangle is composed of 4^ℓ triangle elements while the mesh of the reference square is composed $2\times4^\ell$ triangle

elements. Therefore, on Y, we place $24 \times 4^\ell$ triangle elements on the refinement level ℓ. The resulting macro parametrization and mesh of the domain Y is displayed in Figure 4.1.

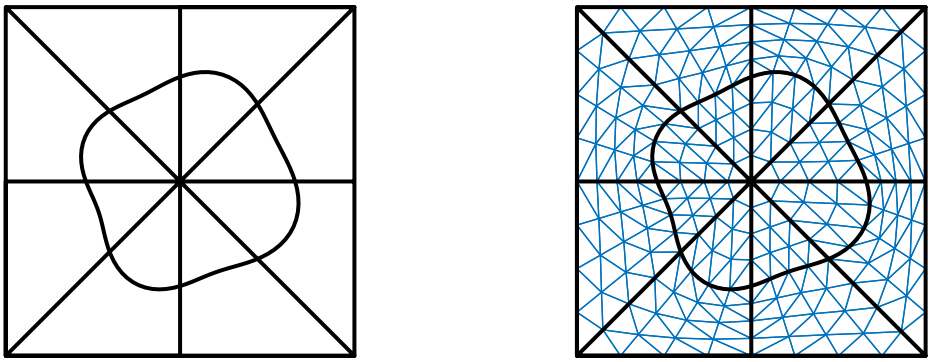

FIG. 4.1. Left-hand side: Parametric representation of Y by quadrangular and triangular patches for resolving the interface exactly. Right-hand side: Mesh on Y on refinement level $\ell = 2$.

Based on the variational formulation of the cell problem (2.11), we define the bilinear form and the linear form

$$B(\boldsymbol{u},\boldsymbol{v}) \coloneqq \int_Y \big(\boldsymbol{A}(\boldsymbol{y}) : \boldsymbol{u}(\boldsymbol{y})\big) : \nabla \boldsymbol{v}(\boldsymbol{y})\,\mathrm{d}\boldsymbol{y}, \quad L(\boldsymbol{v}) \coloneqq -\int_Y \big(\boldsymbol{A}(\boldsymbol{y}) : e_{ij}\big) : \nabla \boldsymbol{v}(\boldsymbol{y})\,\mathrm{d}\boldsymbol{y}, \tag{4.3}$$

respectively, where $\boldsymbol{u}, \boldsymbol{v} \in [H^1_{\mathrm{per}}(Y)]^2$. The kernel of the bilinear function B contains the functions which are constant in one dimension and vanish in the other dimension, i.e. $\boldsymbol{r}_1(\boldsymbol{y}) \coloneqq (1,0)^\intercal$ and $\boldsymbol{r}_2(\boldsymbol{y}) \coloneqq (0,1)^\intercal$. In order to make our problem well-posed, we use Lagrange multipliers: We want to find $\boldsymbol{u} \in [H^1_{\mathrm{per}}(Y)]^2$, such that

$$B(\boldsymbol{u},\boldsymbol{v}) + \sum_{i=1}^{2} \lambda_i \langle \boldsymbol{r}_i, \boldsymbol{v}\rangle = L(\boldsymbol{v}) \text{ for all } \boldsymbol{v} \in [H^1_{\mathrm{per}}(Y)]^2,$$

subject to $\langle \boldsymbol{r}_i, \boldsymbol{u}\rangle = 0$ for $i = 1, 2$. As we have $B(\boldsymbol{r}_i, \boldsymbol{r}_i) = 0$ and $L(\boldsymbol{r}_i) = 0$ for $i = 1, 2$, we can replace λ_i by the constraint and obtain: seek $\boldsymbol{u} \in [H^1_{\mathrm{per}}(Y)]^2$, such that

$$B(\boldsymbol{u},\boldsymbol{v}) + \sum_{i=1}^{2} \langle \boldsymbol{r}_i, \boldsymbol{u}\rangle\langle \boldsymbol{r}_i, \boldsymbol{v}\rangle = L(\boldsymbol{v}) \text{ for all } \boldsymbol{v} \in [H^1_{\mathrm{per}}(Y)]^2.$$

For this modified problem, we use piecewise linear finite elements to find an approximation to the solution of the cell problem (2.7). Since the interface is resolved by the triangulation, the convergence order of our implementation is of second order in the mesh size h with respect to the $[L^2(Y)]^n$-norm.

4.2. **Verification of the shape derivative through finite differences.** Choose $N \in \mathbb{N}$ and let the coefficients $(a_{-N}, \dots, a_0, \dots, a_N) \in \mathbb{R}^{2N+1}$ be describing the interface in our numerical experiments in accordance with (4.1) and (4.2). We use the computable and symmetric expression $(\delta a^*_{ijkl}(\omega)[\boldsymbol{h}] + \delta a^*_{jilk}(\omega)[\boldsymbol{h}])/2$ from Remark 4 to evaluate the shape derivative of the coefficients of the homogenized tensor. As deformation functions, we use the functions

$$\boldsymbol{q}_k(\phi) := \begin{pmatrix} \cos(\phi) \\ \sin(\phi) \end{pmatrix} \times \begin{cases} \sin(k\phi), & \text{if } -N \leq k < 0, \\ \cos(k\phi), & \text{if } 0 \leq k \leq N. \end{cases}$$

Thus, we obtain the shape derivative of the coefficients of the homegenized elasticity tensor with respect to the $2N+1$ directions $\boldsymbol{q}_k$. We compare these $2N+1$ results with an approximation of the shape derivative obtained by first order finite differences. We compute these from the expression (2.8) of the coefficients of the homogenized tensor a^*_{ijkl}, once evaluated on Y with the interface given by the function $r(\phi)$ from (4.2) and once evaluated on Y with the interface given by the function $r(\phi) + \varepsilon \boldsymbol{q}_k(\phi)$. For our test runs, we set $\varepsilon = 10^{-8}$.

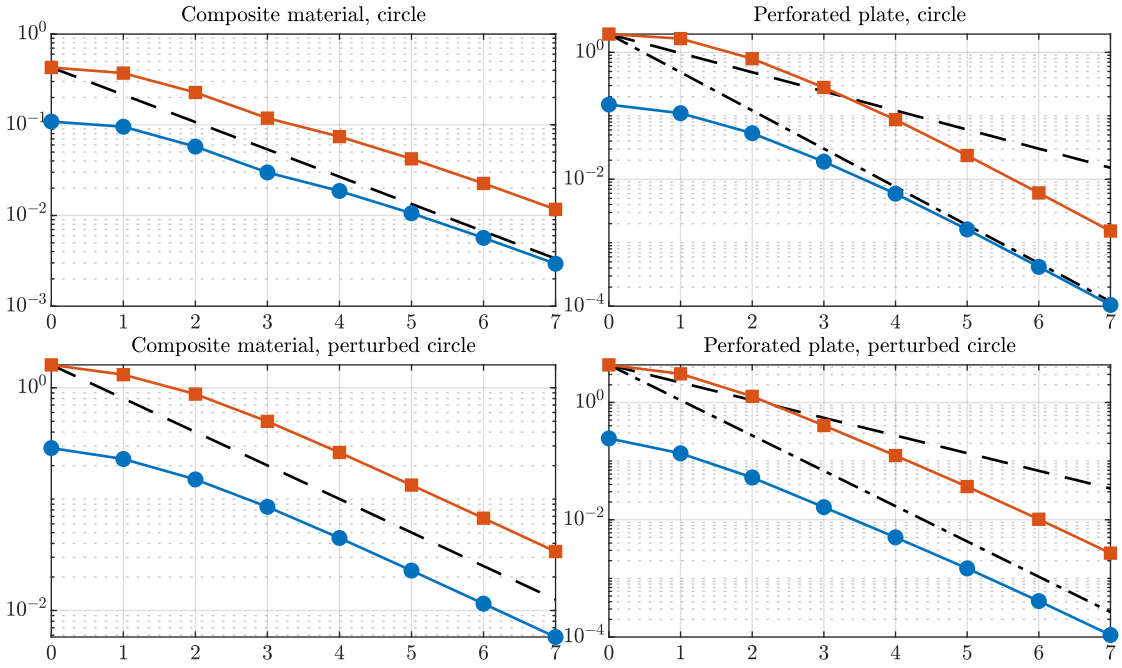

FIG. 4.2. Sum of the ℓ_2-norms of the absolute (—■—) and the relative differences (—●—) between the computable formula (3.11) and the finite difference approximation of the shape derivative in four different settings. The interface is either circular or a slightly perturbed circle, composite and hollow materials are considered, and the mesh refinement levels ℓ of the finite element method range from 0 to 7. As a means of comparison, the plots of linear (– – –) and quadratic decay (-·-·-) are shown where needed.

The material properties are chosen as follows. To realize a composite material, we define the elasticity tensor outside of the interface by the values $E = 1\,\mathrm{Pa}$ and $\nu = 0.3$ and inside of the interface by $E = 2\,\mathrm{Pa}$ and $\nu = 0.2$. Whereas, to obtain a perforated plate, we use $E = 1\,\mathrm{Pa}$ and $\nu = 0.3$ outside of the interface and no material inside of the interface, compare (2.4). The boundary under consideration is a circle of radius $1/4$ on one hand and a respective perturbed version of this circle on the other hand, the same perturbed circle as shown in the mesh plots in Figure 4.1.

In Figure 4.2, the convergence of the evaluation of the formula (2.8) towards the respective finite difference can be observed in all of the four cases. Therefore, we can conclude that our implementation is correct.

5. Numerical results

We use the expressions (3.12) and (3.14) in order to compute the shape derivative of the objective function (2.13) inside an implementation of the gradient descent method. The aim of the procedure is to find optimal interface shapes which minimize the objective function (2.13) for different settings. In the examples below, we choose $N = 32$ in (4.2). The algorithm was always stopped after 75 gradient steps. The results of five settings within a composite material and one within a perforated plate are presented below. The computation of these examples are based on 98 304 and 65 536 finite elements for composite materials and for perforated plates, respectively, which corresponds to the mesh refinement level $\ell = 6$ in our implementation. In all six setting, the materials under consideration are defined by $E_1 \coloneqq 2\,\mathrm{Pa}$ and $\lambda_1 \coloneqq 0.3$ outside of the interface, and in the case of composite materials as $E_2 \coloneqq 5\,\mathrm{Pa}$ and $\lambda_2 \coloneqq 0.2$ inside the interface. The other material parameters are then specified in the respective setting.

5.1. **First example: Anisotropic tensor for a composite material.** In our first experiment, we compute the homogenized tensor $\boldsymbol{A}$ for a composite material, where the interface is described by the circle of radius $1/4$. Then, for the desired homogenized elastictiy tensor $\boldsymbol{B}$, we introduce an anisotropy into $\boldsymbol{A}$ by adapting the two values $b_{1111} \coloneqq a_{1111} + \delta/2$ and $b_{2222} \coloneqq a_{2222} - \delta/2$. With the starting profile chosen to be the circle of radius $1/4$, we apply the gradient descent method for different values of δ. The optimized shapes we found are shown in Figure 5.1. The values of the objective function (rows entitled "$J(\omega)$") and the ℓ_2-norm of the shape gradient (rows entitled "ℓ_2") at the start and at the end of the optimization process are listed in Table 1.

		$\delta = -0.06$	$\delta = -0.04$	$\delta = -0.02$	$\delta = 0$	$\delta = 0.02$	$\delta = 0.04$	$\delta = 0.06$
$J(\omega)$	Start	$9.0 \cdot 10^{-4}$	$4.0 \cdot 10^{-4}$	$1.0 \cdot 10^{-4}$	0	$1.0 \cdot 10^{-4}$	$4.0 \cdot 10^{-4}$	$9.0 \cdot 10^{-4}$
	End	$7.8 \cdot 10^{-7}$	$9.6 \cdot 10^{-8}$	$6.1 \cdot 10^{-9}$	0	$6.1 \cdot 10^{-9}$	$1.2 \cdot 10^{-7}$	$9.7 \cdot 10^{-7}$
ℓ_2	Start	$3.1 \cdot 10^{-2}$	$2.0 \cdot 10^{-2}$	$1.0 \cdot 10^{-2}$	0	$1.0 \cdot 10^{-2}$	$2.0 \cdot 10^{-2}$	$3.1 \cdot 10^{-2}$
	End	$2.9 \cdot 10^{-4}$	$1.1 \cdot 10^{-4}$	$9.3 \cdot 10^{-6}$	0	$9.0 \cdot 10^{-6}$	$1.6 \cdot 10^{-4}$	$9.1 \cdot 10^{-4}$

Table 1. Example 5.1: Key values of the optimization run.

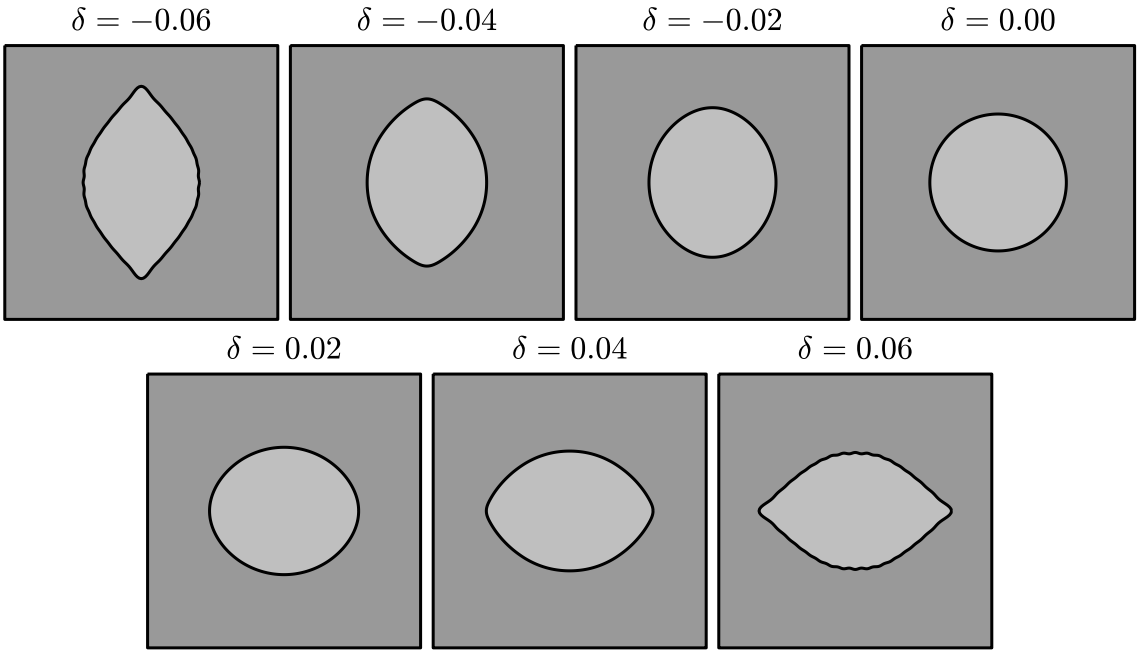

FIG. 5.1. Example 5.1: Optimal shapes in a composite material found for an anisotropic desired elasticity tensor with the anisotropy measured by $\delta = b_{1111} - b_{2222}$, where the initial guess is the circle of radius 1/4.

5.2. **Second example: Anisotropic tensor for a perforated plate.** In this example, we consider perforated plates. We proceed similarly as in the first example to construct the desired homogenized elasticity tensor $\boldsymbol{B}$. We compute the homogenized elasticity tensor $\boldsymbol{A}$ for the circle with radius 1/4 and introduce an anisotropy by setting $b_{1111} = a_{1111} + \delta/2$ and $b_{2222} = a_{2222} - \delta/2$. Again, starting at the circle with radius 1/4, we then apply the gradient descent method to compute the optimal shapes for different values of δ. The optimized shapes we found are shown in Figure 5.2. The values of the objective function and the ℓ_2-norm of the shape gradient at the start and at the end of the optimization process are listed in Table 2.

		$\delta = -1.2$	$\delta = -0.8$	$\delta = -0.4$	$\delta = 0$	$\delta = 0.4$	$\delta = 0.8$	$\delta = 1.2$
$J(\omega)$	Start	$3.6 \cdot 10^{-1}$	$1.6 \cdot 10^{-1}$	$4.0 \cdot 10^{-2}$	0	$4.0 \cdot 10^{-2}$	$1.6 \cdot 10^{-1}$	$3.6 \cdot 10^{-1}$
	End	$1.5 \cdot 10^{-3}$	$2.9 \cdot 10^{-4}$	$1.8 \cdot 10^{-5}$	0	$1.8 \cdot 10^{-5}$	$2.9 \cdot 10^{-4}$	$1.5 \cdot 10^{-3}$
ℓ_2	Start	$1.0 \cdot 10^{1}$	$6.8 \cdot 10^{0}$	$3.4 \cdot 10^{0}$	0	$3.4 \cdot 10^{0}$	$6.8 \cdot 10^{0}$	$1.0 \cdot 10^{1}$
	End	$7.7 \cdot 10^{-3}$	$7.2 \cdot 10^{-3}$	$1.6 \cdot 10^{-3}$	0	$1.6 \cdot 10^{-3}$	$7.2 \cdot 10^{-3}$	$7.7 \cdot 10^{-3}$

TABLE 2. Example 5.2: Key values of the optimization run.

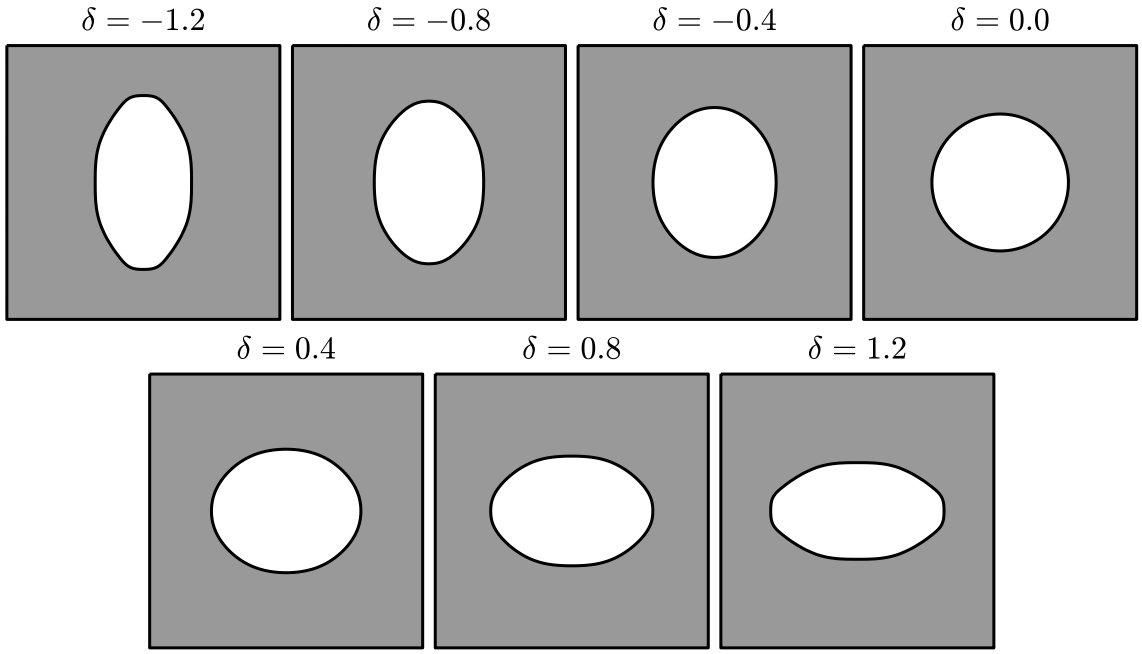

FIG. 5.2. Example 5.2: Optimized shapes in a perforated plate found for an anisotropic desired homogenized elasticity tensor with the anisotropy measured by $\delta = b_{1111} - b_{2222}$, where the initial guess is the circle of radius 1/4.

5.3. **Third example: Various starting profiles for one anisotropic tensor.** In our third experiment, we are concerned with the uniqueness of optimal shapes for the shape optimization problem under consideration. We consider the desired homogenized elasticity tensor to be anisotropic, namely the desired homogenized tensor from Section 5.1 with $\delta = -0.04$. We choose our initial guess to be the circle of radius 1/4 for the first run, an axes-aligned ellipse for the second run, its rotated version for the third run, and finally we randomly perturb the circle for the last run, compare the first row in Figure 5.3. We apply the gradient descent method to optimize the shape for these various initial guesses. The results are shown in the second row of Figure 5.3. The values of the objective function and the ℓ_2-norm of the shape gradient at the start and at the end of the optimization process are listed in Table 3. This example indicates strongly that the solution is not unique as all optimized shapes exhibit both, small values of the objective functional and small norms of the discrete shape gradient. Indeed, the same has already been observed in [6] in case of a second order diffusion equation.

5.4. **Fourth example: Inhomogeneous material inside a composite material.** In the fourth example, we consider the elasticity module $E(\boldsymbol{y})$ and the Poisson ratio $\lambda(\boldsymbol{y})$ to

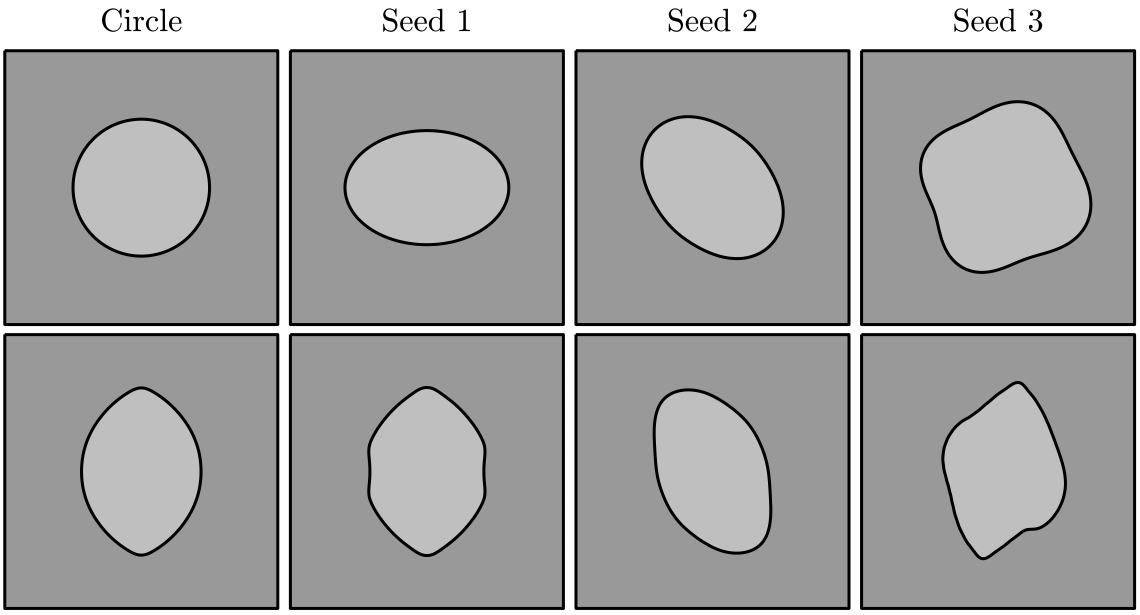

FIG. 5.3. Example 5.3: Starting and optimized shapes found in a composite material for a specific anisotropic desired homogenized elasticity tensor (second row), where the various initial guesses are the circle of radius 1/4 and random perturbations of this circle (first row).

		Circle	Seed 1	Seed 2	Seed 3
$J(\omega)$	Start	$4.0 \cdot 10^{-4}$	$1.9 \cdot 10^{-3}$	$4.2 \cdot 10^{-4}$	$4.5 \cdot 10^{-2}$
	End	$9.6 \cdot 10^{-8}$	$1.2 \cdot 10^{-7}$	$3.0 \cdot 10^{-7}$	$1.8 \cdot 10^{-7}$
ℓ_2	Start	$2.0 \cdot 10^{-2}$	$5.7 \cdot 10^{-2}$	$2.0 \cdot 10^{-2}$	$2.0 \cdot 10^{0}$
	End	$1.1 \cdot 10^{-4}$	$2.0 \cdot 10^{-4}$	$1.9 \cdot 10^{-5}$	$2.8 \cdot 10^{-4}$

TABLE 3. Example 5.3: Key values of the optimization run.

be nonconstant functions in the interior of the interface, namely

$$E(\boldsymbol{y}) \coloneqq E_2 \frac{1 + \sin(\pi y_1) + \sin(\pi y_2)}{2} \quad \text{and} \quad \lambda(\boldsymbol{y}) \coloneqq \lambda_2 e^{-(2y_1-1)^2-(2y_2-1)^2}. \tag{5.1}$$

In the exterior of the interface, we keep the same homogeneous material properties as in the previous examples, given by E_1 and λ_1. We moreover use the anisotropic desired homogenized tensor from Section 5.1 with $\delta = -0.04$ as desired homogenized elasticity tensor $\boldsymbol{B}$. We take the four different initial guesses from Section 5.3 and apply the gradient descent method. We obtain for these initial guesses the optimized shapes shown in Figure 5.4. The values of the objective function and the ℓ_2-norm of the shape gradient at the start and at

the end of the procedure are listed in Table 4. Again, the optimal shape seems not to be unique.

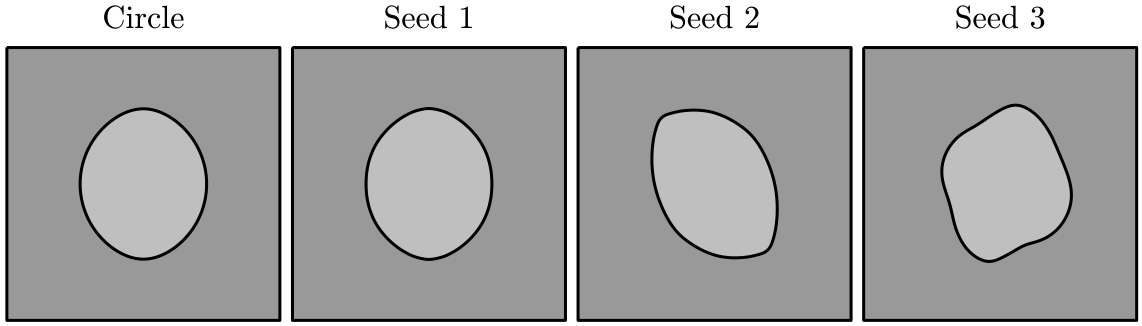

FIG. 5.4. Example 5.4: The composite material is defined by E_1 and λ_1 outside and a heterogeneous material on the inside of the interface, described by the functions $E(\boldsymbol{y})$ and $\lambda(\boldsymbol{y})$ from (5.1). Optimized shapes found for an anisotropic desired homogenized elasticity tensor are shown, where the initial guesses as in Figure 5.3 have been used.

		Circle	Seed 1	Seed 2	Seed 3
$J(\omega)$	Start	$4.0 \cdot 10^{-4}$	$4.1 \cdot 10^{-3}$	$4.6 \cdot 10^{-4}$	$8.0 \cdot 10^{-2}$
	End	$4.0 \cdot 10^{-9}$	$1.5 \cdot 10^{-8}$	$4.9 \cdot 10^{-7}$	$1.5 \cdot 10^{-6}$
ℓ_2	Start	$3.8 \cdot 10^{-2}$	$1.5 \cdot 10^{-1}$	$4.1 \cdot 10^{-2}$	$3.5 \cdot 10^{0}$
	End	$5.0 \cdot 10^{-5}$	$1.1 \cdot 10^{-4}$	$1.7 \cdot 10^{-4}$	$2.0 \cdot 10^{-4}$

TABLE 4. Example 5.4: Key values of the optimization run.

5.5. **Fifth example: Convergence towards specific material properties.** In this example, we choose the desired homogenized tensor to represent a material which has elasticity module $\tilde{E} \coloneqq 1.15\,\mathrm{Pa}$ and Poisson ratio of $\tilde{\lambda} \coloneqq 0.285$. These values were chosen such that $E_1 < \tilde{E} < E_2$ and $\lambda_2 < \tilde{\lambda} < \lambda_1$. With the same initial guesses as in Section 5.3, we obtain the optimized shapes found in Figure 5.5. The values of the objective function and the ℓ_2-norm of the shape gradient at the start and at the end of the procedure are given in Table 5.

5.6. **Sixth example: Convergence towards inverted composite material.** In this example, the desired homogenized tensor represents a composite material which has material properties E_1 and λ_1 inside and E_2 and λ_2 outside of the interface. This correponds to a setting where the two materials of the composite materials we considered yet have switched their position. In order to define the desired homogenized elasticity tensor $\boldsymbol{B}$, we consider a circle with radius of 0.48. This ensures that an attainable desired tensor is derived. We use the same initial guesses as in Section 5.3, which yields the optimized

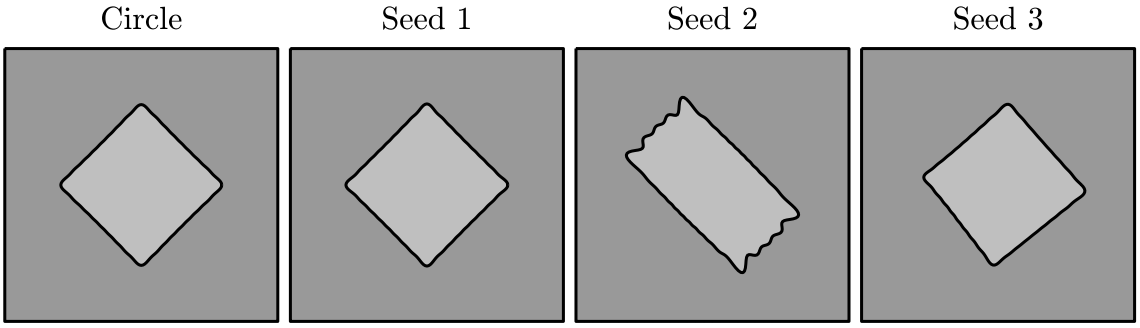

FIG. 5.5. Example 5.5: Optimal shapes found for a desired tensor, describing the material with elasticity module $\tilde{E} = 1.15\,\mathrm{Pa}$ and Poisson ratio $\tilde{\lambda} = 0.285$. The initial guesses are the ones shown in the first row of Figure 5.3.

		Circle	Seed 1	Seed 2	Seed 3
$J(\omega)$	Start	$1.6 \cdot 10^{-3}$	$2.4 \cdot 10^{-3}$	$1.4 \cdot 10^{-3}$	$6.0 \cdot 10^{-2}$
	End	$2.9 \cdot 10^{-4}$	$2.9 \cdot 10^{-4}$	$1.8 \cdot 10^{-4}$	$3.1 \cdot 10^{-4}$
ℓ_2	Start	$2.3 \cdot 10^{-1}$	$2.6 \cdot 10^{-1}$	$2.3 \cdot 10^{-1}$	$2.3 \cdot 10^{0}$
	End	$7.7 \cdot 10^{-4}$	$4.0 \cdot 10^{-4}$	$1.7 \cdot 10^{-3}$	$1.7 \cdot 10^{-3}$

TABLE 5. Example 5.5: Key values of the optimization run.

shapes found in Figure 5.6. The respective values of the objective function and the ℓ_2-norm of the shape gradient at the start and at the end of the optimization process are listed in Table 6.

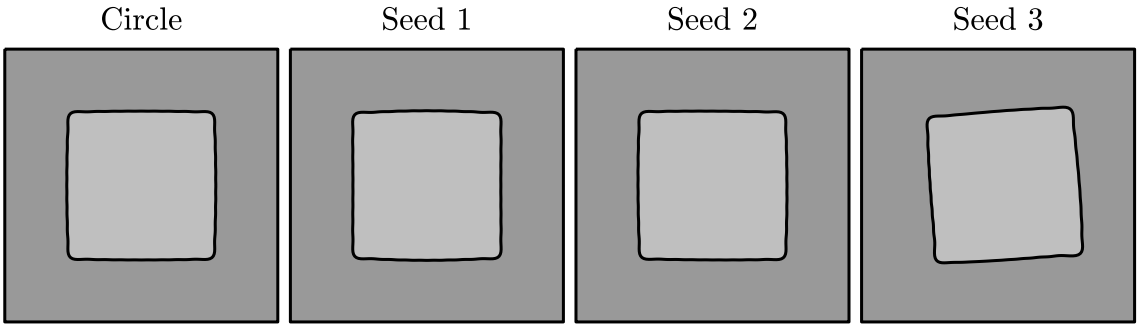

FIG. 5.6. Example 5.6: Optimal shapes found for a desired homogenized elasticity tensor, by switching the position of the materials in respect to the interface. The initial guesses are the ones shown in the first row of Figure 5.3.

		Circle	Seed 1	Seed 2	Seed 3
$J(\omega)$	Start	$5.8 \cdot 10^{-2}$	$5.8 \cdot 10^{-2}$	$5.9 \cdot 10^{-2}$	$1.6 \cdot 10^{-3}$
	End	$2.0 \cdot 10^{-4}$	$2.0 \cdot 10^{-4}$	$2.0 \cdot 10^{-4}$	$2.1 \cdot 10^{-4}$
ℓ_2	Start	$1.7 \cdot 10^{0}$	$1.7 \cdot 10^{0}$	$1.7 \cdot 10^{0}$	$2.6 \cdot 10^{-1}$
	End	$1.1 \cdot 10^{-4}$	$9.1 \cdot 10^{-4}$	$2.6 \cdot 10^{-4}$	$2.4 \cdot 10^{-3}$

TABLE 6. Example 5.6: Key values of the optimization run.

6. Conclusion

In this article, shape sensitivity analysis of the effective tensor in case of periodic materials has been performed. In particular, we computed the Hadamard representation of the shape derivative of the least square matching of a desired material tensor. Numerical experiments by means of a finite element implementation in the two-dimensional setting have been presented for composite materials and for perforated plates. Likewise to [6], it has been observed that the computed optimal shapes depend on the initial guess, which means that the solution of the problem under consideration seems to be in general not unique. We emphasize, however, that a volume constraint as in the case of compliance optimization is not necessary – the optimization algorithm stagnates in the (nonunique) minimum.

References

[1] T. Adachi, Y. Osako, M. Tanakaa, M. Hojo, and S.J. Hollister. Framework for optimal design of porous scaffold microstructure by computational simulation of bone regeneration. *Biomaterials* **27** (2006) 3964–3972.

[2] G. Allaire. *Shape Optimization by the Homogenization Method*. Springer, New York, 2002.

[3] G. Allaire, P. Geoffroy-Donders, and O. Pantz. Topology optimization of modulated and oriented periodic microstructures by the homogenization method. *Comput. Math. Appl.* **78**(7) (2019) 2197–2229.

[4] D. Braess. *Finite Elements. Theory, Fast Solvers, and Applications in Solid Mechanics*. Cambridge University Press, Cambridge, 2001.

[5] L. Colabella, A.P. Cisilino, V. Fachinotti, and P. Kowalczyk. Multiscale design of elastic solids with biomimetic cancellous bone cellular microstructures. *Struct. Multidiscip. Optim.* **60** (2019) 639–661.

[6] M. Dambrine and H. Harbrecht. Shape optimization for composite materials and scaffolds. *Multiscale Model. Sim.* **18**(2) (2020) 1136–1152.

[7] M. Delfour and J.-P. Zolesio. *Shapes and Geometries*. SIAM, Philadelphia, 2001.

[8] A. Ferrer, J.C. Cante, J.A. Hernández, and J. Oliver. Two-scale topology optimization in computational material design: An integrated approach. *Int. J. Numer. Meth. Eng.* **114** (2018) 232–254.

[9] P. Geoffroy-Donders. *Homogenization Method for Topology Optimization of Structures built with Lattice Materials*. PhD thesis, Ecole Polytechnique, France, 2018.

[10] H. Harbrecht, M. Multerer, and R. von Rickenbach. Isogeometric shape optimization for scaffold structures. arXiv:2105.15158, 2021.

[11] S.J. Hollister, R.D. Maddox, and J.M. Taboas. Optimal design and fabrication of scaffolds to mimic tissue properties and satisfy biological constraints. *Biomaterials* **23** (2002) 4095–4103.

[12] D. Hübner, E. Rohan, V. Lukeš, and M. Stingl. Optimization of the porous material described by the Biot model. *Int. J. Solids Struct.* **156–157** (2019) 216–233.

[13] R. Huiskes, H. Weinans, H.J. Grootenboer, M. Dalstra, B. Fudala, and T.J. Slooff. Adaptive bone-remodeling theory applied to prosthetic-design analysis. *J. Biomechanics* **20** (1987) 1135–1150.
[14] C.Y. Lin, N. Kikuchia, and S.J. Hollister. A novel method for biomaterial scaffold internal architecture design to match bone elastic properties with desired porosity. *J. Biomechanics* **37** (2004) 623–636.
[15] D. Luo, Q. Rong, and Q. Chen. Finite-element design and optimization of a three-dimensional tetrahedral porous titanium scaffold for the reconstruction of mandibular defects. *Med. Eng. Phys.* **47** (2017) 176–183.
[16] M. Itskov. *Tensor Algebra and Tensor Analysis for Engineers*. Springer, Berlin, 2007.
[17] F. Murat and J. Simon. Étude de problèmes d'optimal design. In *Optimization techniques, modeling and optimization in the service of man*, edited by J. Céa, Lect. Notes Comput. Sci. 41, Springer, Berlin, 54–62 (1976).
[18] G. Nika and A. Constantinescu. Design of multi-layer materials using inverse homogenization and a level set method. *Comput. Methods Appl. Mech. Engrg.* **346** (2019) 388–409.
[19] D.K. Pattanayak, A. Fukuda, T. Matsushita, M. Takemoto, S. Fujibayashi, K. Sasaki, N. Nishida, T. Nakamura, and T. Kokubo. Bioactive Ti metal analogous to human cancellous bone. Fabrication by selective laser melting and chemical treatments. *Acta Biomaterialia* **7** (2011) 1398–1406.
[20] O. Pironneau. *Optimal Shape Design for Elliptic Systems*. Springer, New York, 1984.
[21] G. Rotta, T. Seramak, and K. Zasińska. Estimation of Young's modulus of the porous titanium alloy with the use of FEM package. *Adv. Mat. Sci.* **15** (2015) 29–37
[22] F. Schury, M. Stingl, and F. Wein. Efficient two-scale optimization of manufacturable graded structures. *SIAM J. Sci. Comput.* **34** (2012) B711–B733.
[23] O. Sigmund. Tailoring materials with prescribed elastic properties. *Mech. Mat.* **20** (1995) 351–368.
[24] J. Sokolowski and J.-P. Zolesio. *Introduction to Shape Optimization: Shape Sensitivity Analysis*. Springer, 1992.
[25] Y. Wang and Z. Kang. Concurrent two-scale topological design of multiple unit cells and structure using combined velocity field level set and density mode. *Comput. Methods Appl. Mech. Engrg.* **347** (2019) 340–364.
[26] X. Wang, S. Xu, S. Zhou, W. Xu, M. Leary, P. Choong, M. Qian, M. Brandt, and Y.M. Xie. Topological design and additive manufacturing of porous metals for bone scaffolds and orthopaedic implants: A review. *Biomaterials* **83** (2016) 127–141.
[27] M. Wormser, F. Wein, M. Stingl, and C. Körner. Design and additive manufacturing of 3D phononic band gap structures based on gradient based optimization. *Materials* **10** (2017) 1125.
[28] A. Zenisek. *Nonlinear Elliptic and Evolution Problems and Their Finite Element Approximation.* Academic Press, San Diego, 1990.

Departement für Mathematik und Informatik, Universität Basel, Spiegelgasse 1, 4051 Basel, Switzerland

Email address: {merlin.fallahpour,helmut.harbrecht}@unibas.ch